




Dislocation-based high-temperature plasticity of polycrystalline perovskite SrTiO_3

Lukas Porz^{1,*} , Michael Scherer¹, Marion Höfling², Atsutomo Nakamura^{3,4}, Wolfgang Rheinheimer⁵, and Jürgen Rödel¹

¹Department of Materials and Earth Sciences, Technical University of Darmstadt, Darmstadt, Germany

²Department of Physics, Technical University of Denmark, Kgs. Lyngby, Denmark

³Department of Mechanical Science and Bioengineering, Osaka University, Osaka, Japan

⁴Japan Science and Technology Agency, PRESTO, Saitama, Japan

⁵Institute for Energy and Climate Research – Materials Synthesis and Processing, Forschungszentrum Jülich GmbH, Jülich, Germany

Received: 20 February 2022

Accepted: 2 June 2022

Published online:

23 January 2023

© The Author(s) 2023

ABSTRACT

Dislocation networks have been demonstrated to substantially enhance functional properties. As-sintered samples are virtually devoid of dislocations, new innovative techniques for introducing sufficiently high dislocation densities into polycrystalline ceramics are needed. While dislocation-based plasticity at high temperatures has been demonstrated for a large range of ceramic single crystals, plasticity in polycrystals is much less understood. Here, we demonstrate plastic strains in excess of several % based on dislocation motion in polycrystalline SrTiO_3 at $\approx 1100^\circ\text{C}$ with $3.9\ \mu\text{m}$ grain size. Ultra-high voltage electron microscopy reveals an associated increase in dislocation density by three orders of magnitude. Achievable strain rates are comparable to creep-based mechanisms and much less sensitive to applied stress than observed for metals. A specialized testing protocol allows quantification of the deformability via stress exponent, activation volume and activation enthalpy giving additional quantification. In conjunction with TEM images, the mechanical data gives insight into the underlying mechanisms.

Introduction

Dislocations are experiencing renewed interest for their potential to tune functional properties [1–3]. Electronic [4, 5], ionic [6, 7] or thermal [8, 9] conductivity and other functionalities can be influenced

by dislocations via their strain field and core charge with its compensating space charge. For perovskites, the influence on mechanical [10] and ferroelectric [11] properties was recently demonstrated. However, efficient insertion of a high density of dislocations into ceramics [12] still remains elusive.

Handling Editor: David Cann.

Address correspondence to E-mail: porz@ceramics.tu-darmstadt.de

In the 1960s and 1970s hot forging experiments were conducted to increase the dislocation density in polycrystalline ceramics [13, 14]. Even though significant potential was elucidated, frequent sample failure remained critical. Additionally, reports from rock deformation in geology at low strain rates underscore the potential in the plasticity of polycrystalline ceramics [15].

Because of decreased complexity, single crystals are more extensively studied. Some exhibit dislocation-based deformability at ambient conditions [16–18] while others require thermal activation [16, 19–21]. In contrast, even though data on the respective single crystals is available, plasticity of polycrystalline ceramics is much less understood for two key reasons: (1) The mechanistic understanding is much more complicated than in single crystals due to the compatibility of the limited number of slip systems [22, 23]. (2) Additional mechanisms, such as diffusion or grain boundary sliding [24, 25] interfere with dislocation plasticity.

Here, we investigate the massive deformability of several % of polycrystalline SrTiO_3 as model perovskite and document a substantial increase in dislocation density during deformation. Achievable strain rates are tested between 1050 °C and 1150 °C to illustrate a suitable parameter range for dislocation-based deformation. Consequent quantitative mapping of the strain rate over large stress ranges allows to quantify the stress exponent, activation volume and activation enthalpy. This data are contrasted to available data from single crystals [16, 19] to give insight into the underlying mechanisms.

Materials and methods

Materials

High-purity stoichiometric strontium titanate was synthesized by the mixed oxide/carbonate route based on SrCO_3 and TiO_2 (purity of 99.95% and 99.995%, Sigma-Aldrich Chemie GmbH, Taufkirchen, Germany). The raw materials were attrition-milled, calcined at 975 °C for 6 h and subsequently milled in a planetary ball mill. Green bodies were cold-isostatically pressed (400 MPa) and sintered at 1425 °C for 1 h in O_2 atmosphere followed by 15 h at 1350 °C in O_2 atmosphere. Resulting specimen were of rel.

density > 99.5% with a mean grain size of $3.9 \pm 0.5 \mu\text{m}$ [26].

It was documented that this processing results in single-phase, high-purity polycrystals [27]. Particularly, the grain boundaries were shown to be free of any amorphous layers or other secondary phases [28]. Even from small impurity concentrations, such as 0.1% [24, 29], secondary phases can form at the grain boundaries which can lead to grain boundary sliding and sample failure during high-temperature deformation.

The base surfaces of the cylindrical samples were ground plane-parallel to a height of 8 mm with a grinding machine, while the diameter was reduced to 4 mm using a lathe. As a precaution to minimize residual stresses from post-processing, the samples were annealed in air at 400 °C for 2 h before deformation.

Deformation

For deformation, a load frame (Z010, Zwick GmbH & Co. KG, Ulm, Germany) equipped with centered alumina rods for sample contacting, was used. The alumina rods were surrounded by a clamshell furnace (LK/ SHC 1500-85-150-1-V-Sonder, HTM Reetz GmbH, Berlin, Germany). The sample displacement was quantified with a linear variable differential transducer (LVDT) system with a nominal accuracy of 10 nm and final height reduction in the sample selectively confirmed ex situ with a μm gauge. To assure a uniaxial stress state, the sample was centered carefully. Additionally, a hemispherical cap was placed on top of the sample to minimize tilting.

The chosen temperature range between 1050 °C and 1150 °C was determined by the operation limit for superalloys that could be used as forming tools for hot-working of polycrystalline ceramics and data available from single crystals [16, 30, 31]. In order to obtain a deformation map with some predictability for other stresses and strain rates, a large spread of strain rates was aspired using step-wise loading, ranging from 20 to 300 MPa. As a result, strain rate levels down to below $3 \times 10^{-8} \text{ s}^{-1}$ (which approaches the instrumentation limit of the LVDT) could be quantified and up to above $2 \times 10^{-5} \text{ s}^{-1}$ could be obtained. All tests were done with a heating rate of 5 Kmin^{-1} and a pre-load of 1.5 MPa. The temperature was equilibrated for 20 min when reaching the experiment's temperature. Cooling to room

temperature was done with no load applied. Throughout the manuscript, the stresses are defined as absolute values in compression direction.

For each temperature, the stress levels were recorded with the same sample in a series from low to high stresses and consequentially at 1100 °C and 1050 °C. The data for 1150 °C were recorded twice in a row on the same sample to confirm that deformation history has no significant impact. Hence, all data in the strain rate map stems from one sample. The time for which the load was held constant was chosen as best compromise for each load and temperature so that the degree of deformation in each step was kept small but large enough to assure getting into the regime of constant strain rate.

Electron microscopy

An ultra-high voltage electron microscope was utilized in scanning transmission electron microscopy (STEM) mode. The acceleration voltage was set to 1 MeV in BF-STEM imaging mode using the JEOL JEM-1000 k RS (JEOL, Tokyo, Japan). This high acceleration voltage allows observing relatively thick sample sections and large sample areas. An as-sintered sample was contrasted to a 4.2% deformed one. Conventional polishing and ion milling was used for sample preparation. The dislocation density was quantified by the number of lines per unit area as averaged over 10 grains.

Results

Preliminary experiments and testing strategy

To test the boundary conditions, preliminary experiments clarified two aspects:

(1) Diffusion was ruled out as deformation mechanism under uniaxial compression. Nabarro-Herring or Coble creep would yield a dependence of the grain size d of order $1/d^2$ and $1/d^3$, respectively, for the strain rate $\dot{\epsilon}$. Instead, strain rates decrease with decreasing grain size, as exemplary depicted in Supplemental 1.

(2) Deformation history showed a negligible effect and sample failure was not observed in the first few percent of deformation with 28% strain as maximum value tested, as presented in Supplemental 2.

This allows us to safely apply the standardized protocol, presented in Fig. 1a, for quantifying the deformability.

During the step-wise increased constant stresses, the sample displacement was recorded. Based on the displacement, true strain is calculated. The applied compressive stress and recorded strain is given as function of time in Fig. 1. A closer observation of Fig. 1b verifies that after several seconds, indicated by a linear behavior, steady-state compression is reached and the slope can be fitted linearly as the resulting strain rate for the respective stress. In order to capture the temperature dependence, three different temperatures were investigated. After recording all data points at 1150 °C, data points of the same stress levels were consecutively recorded for 1100 °C and 1050 °C on the same sample. By adjusting the time interval of constant load, it was possible to restrict all data points to a deformation of around 0.1% per step. By doing so, the cumulative deformation over all temperatures and all stresses was kept to 2–5% in reference experiments (see Supplemental 3) and 3.2% in the presented case to avoid geometry changes.

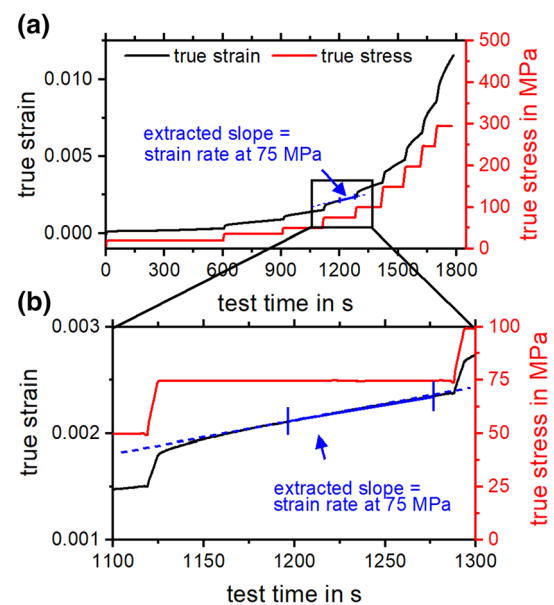


Figure 1 Step-wise deformation of polycrystalline SrTiO₃. **a** Strain signal recorded during the deformation at 1150 °C using step-wise increased stress plateaus. **b** Magnification of a constant stress section of (a) illustrating a fit of strain rate from the linear regime.

Quantification of plasticity

Stress and temperature dependence of the achievable strain rate was mapped over different stress levels and temperatures as displayed in Fig. 2. Data points are collected over a large stress regime covering both low and high stresses according to Fig. 1. This data are featured in Fig. 2 both in double-logarithmic and in semi-logarithmic form allowing analysis from two different perspectives.

The double-logarithmic presentation in Fig. 2a allows extraction of the stress exponent n . It links the strain rate $\dot{\epsilon}$ to the applied stress σ via Eq. 1. [32] B is a pre-factor, ΔG the activation energy, k_B the Boltzmann constant and T is the temperature. A stress exponent of $n \approx 1.7$ is found for all temperatures.

$$\dot{\epsilon} = B\sigma^n \exp\left(-\frac{\Delta G}{k_B T}\right) \quad (1)$$

A semi-logarithmic form of presentation of the data affords interpretation from a different perspective. The plot in Fig. 2b reveals a steep slope below approximately 75 MPa, where small increases in stress raise the observed strain rate. Above 75 MPa, a linear dependence indicated with a dashed black line is found where additional stress only slightly increases the strain rate.

Moreover, the presentation form in Fig. 2b allows to extract the activation volume V . It quantifies the dependence of strain rate on the applied stress and

gives insight into how easily the deformation can be accelerated by additional stress [16]. In an alternate description to Eq. 1, Eq. 2 links the strain rate to activation energy ΔG consisting of activation volume V and activation enthalpy ΔH .

$$\dot{\epsilon} = \dot{\epsilon}_0 \cdot \exp\left(-\frac{\Delta G}{k_B \cdot T}\right) = \dot{\epsilon}_0 \cdot \exp\left(-\frac{\Delta H - V \cdot \tau^*}{k_B \cdot T}\right) \quad (2)$$

Specifically, the activation volume V is the slope of the strain rate $\dot{\epsilon}$ on uniaxial stress, respectively shear stress τ , at a specific temperature T including the Boltzmann constant k_B [12, 16] following Eq. 3:

$$V(\tau) = k_B T \left[\frac{\partial \ln(\dot{\epsilon} \cdot 1s)}{\partial \tau} \right]_T \quad (3)$$

The results are presented in Fig. 3a as function of applied stress. The y-axis is given in three different units, i.e., in 10^{-27} m^3 , $b_{<110>\{110\}}^3$ and $b_{<100>\{100\}}^3$ while the x-axis is given in uniaxially applied stress σ .

Furthermore, the temperature dependence of the strain rate is quantified with an activation enthalpy using the relation provided in Eq. 2 (Fig. 3b). Extrapolation of the high-stress value $\approx 5.9 \text{ eV}$ to zero stress yields the activation energy ΔG in good approximation. More advanced descriptions and reasoning for underlying approximations can be found elsewhere. [12]

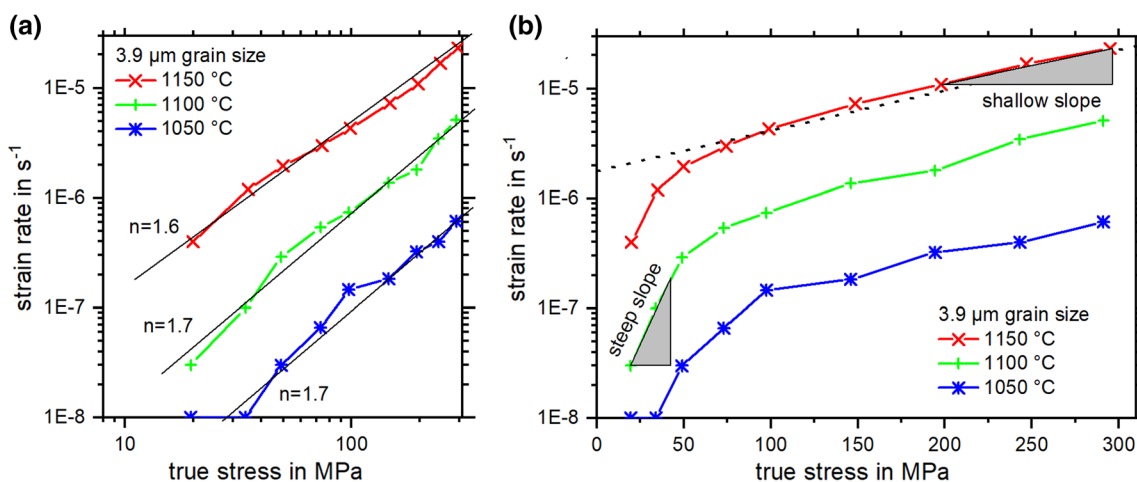


Figure 2 Strain rate for the deformation of polycrystalline SrTiO₃ plotted in dependence of stress. Data points have been extracted for step-wise constant stresses between 20 and 300 MPa according to the procedure presented in Fig. 1 for one sample for 1150 °C, 1100 °C and 1050 °C (in that order) with an accumulative strain of

3.2%. **a** Presentation in double-logarithmic form with extraction of the stress exponent n . **b** Presentation in semi-logarithmic form allowing the extraction of the activation volume. Here, a regime with steep slope at low loads and a regime with a shallow slope at high loads is visible.

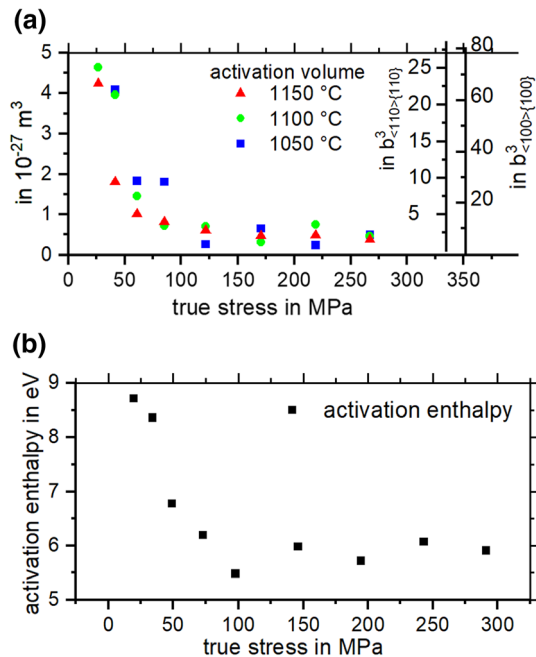


Figure 3 Quantification of activation volume and activation enthalpy. **a** Activation volume at different stress levels plotted in dependence of the uniaxially applied stress. The y-axis scales for absolute values and is simultaneously given as multiples of the cubic Burgers vectors of the two relevant slip systems. **b** Activation enthalpy extracted from data presented in Fig. 2b.

Ultra-high voltage electron microscopy

As-sintered samples featured a dislocation density of $6 \times 10^9 \text{ m}^{-2}$ [9], with three dislocations in 133 grains found [10], see Fig. 4a. In contrast, a sample deformed to 4.2% strain revealed a dislocation density of $3 \times 10^{12} \text{ m}^{-2}$ [12] signifying an increase by three orders of magnitude. However, the dislocation density was found to only increase to $6 \times 10^{12} \text{ m}^{-2}$ at 10.2% strain suggesting minor changes after initial

deformation. While some grains appear to remain dislocation-free, the large majority contained abundant dislocations with a multitude of morphologic features, such as curved or faceted lines, small loops, and areas with high and low dislocation density.

Discussion

The most eye-catching behavioral feature observed is the insensitivity of the strain rate on the applied stress which is in strong contrast to the behavior of metals [32]. Even tripling the applied stress from 100 to 300 MPa accelerates the deformation only by a factor of five. In other words, the stress exponent $n \approx 1.7$ is extremely low compared to values of $n = 10$ to $n = 1000$ found for room temperature plasticity of fcc metals [12].

Hence, a certain strain rate range cannot be exceeded by further increasing the stress. In turn, sample failure may occur when deformation is strain rate-controlled and the strain rate is chosen too high for the respective temperature [33–35]. Additionally, Singh et al. report diffusion and grain boundary sliding-based deformation with stress exponents of $n = 0.9$ to $n = 1.6$ for SrTiO_3 at low stresses. [29]

In our experiment, we avoided sample failure by setting a stress and obtaining strain rate as response instead of setting a strain rate and face not manageable stress levels. Additionally, as discussed in the following, we find that increasing the temperature – which has technical limitations – can substantially enhance the velocity of the dislocations and therefore the strain rate.

The average velocity of the dislocations can be taken from the Orowan Eq. (4) [36, 37] which

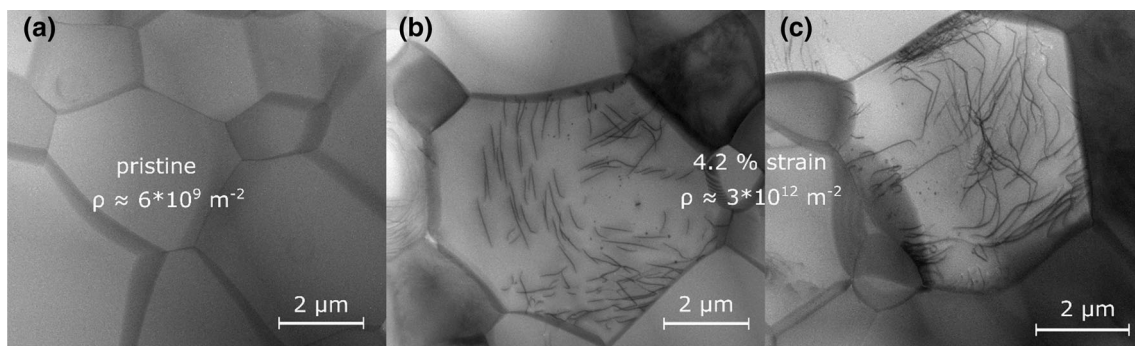


Figure 4 Ultra-high voltage electron microscopy images of polycrystalline SrTiO_3 . **a** After sintering, **b** and **c** after 4.2% deformation with visible dislocations.

connects it to the macroscopic strain rate $\dot{\epsilon}$, the dislocation density ρ , the Burgers vector b and the effective Schmid factor m_s which is used to convert the shear rate $\dot{\gamma}$ to the measured strain rate $\dot{\epsilon}$.

$$v_d = \frac{\dot{\epsilon}}{m_s \cdot \rho \cdot b} \quad (4)$$

Using $\dot{\epsilon} = 10^{-5} \text{ s}^{-1}$, $b = 0.55 \text{ nm}$ and $m_s = 0.327$ for 1150°C and 200 MPa yields a dislocation velocity of 28 nm s^{-1} or, in other words, only about 70 unit cells per second. Identifying the exact mechanisms limiting the dislocation velocity and, hence, the deformability of polycrystalline ceramics will be an intriguing challenge. The kink-pair mechanism is one suggested candidate [38, 39].

The strong dependence on temperature and the insensitivity of strain rate on stress are also found in studies on hot forging polycrystalline ceramics from the 1960s and 70s [31, 35, 40–43]. However, these tendencies were neither clearly expressed nor elucidated because mostly creep experiments at low stresses or fixed strain rates or, alternatively, stress–strain curves were used for characterization which cover too narrow a range of stress, strain rate and temperature.

The observed activation parameters may point toward the limiting mechanism. While the set of $\langle 100 \rangle \{100\}$ slip systems is sufficiently mobile at 1100°C [16], it only has three independent slip systems [22] and therefore does not fulfill the Taylor criterion [23]. In consequence, the much less thermally activated set of $\langle 110 \rangle \{110\}$ slip systems [16, 38] must also participate in the deformation. The activation parameters for the latter slip system were reported to be $V \approx 1 b^3_{\langle 110 \rangle \{110\}}$ and $\Delta H = 6 \text{ eV}$ at 1100°C [16]. We observe an activation enthalpy of $\Delta H = 5.9 \text{ eV}$ and an activation volume of $V \approx 2 b^3_{\langle 110 \rangle \{110\}}$ for the polycrystals which matches well the values observed for the $\langle 110 \rangle \{110\}$ slip system in single crystals [16]. Further indications for the rate limitation by the $\langle 110 \rangle \{110\}$ slip system are discussed in supplemental materials 4 and 5. This leads to the hypothesis that the overall deformation is limited by the slowest slip system required to fulfill the Taylor criterion.

To date, substantially more data on dislocation-based plasticity of single crystalline ceramics is available while for the respective polycrystalline material it is often unclear whether it can or cannot

show dislocation based plasticity. This simple example on perovskite SrTiO_3 features dislocation-based hot-deformability of polycrystalline ceramics. As little data were available on polycrystalline plastic deformation of ceramics, beyond creep, we may speculate for still hidden potential in other ceramics as well.

Summary

We report excellent dislocation-based plasticity of several % of polycrystalline perovskite SrTiO_3 at temperatures around 1100°C without sample failure observed. Upon deformation, the dislocation density was found to increase by three orders of magnitude to a range between 10^{12} m^{-2} to 10^{13} m^{-2} . Mapping of the stress- and temperature-dependent strain rate allowed extraction of stress exponent, activation volume and enthalpy for a quantification of the deformability. Most notably, the average dislocation velocity was found to be very small (of the order of tens of nm/s), and an increase in applied stress only marginally increased the strain rate. Faster deformation was only attainable by increasing the temperature. The similarity of activation energy and volume points toward the mobility of the slower $\langle 110 \rangle \{110\}$ slip system being the rate limiting mechanism. The relation of existing data from single crystals to the behavior of polycrystals invites investigation of dislocation-based plasticity of other polycrystalline ceramics where large plastic strains have not been reported to date.

Acknowledgements

We acknowledge assistance from Jan-Helmut Preusker, Nitán Kohli and Daniel Isaia with instrumentation and sample preparation. Karsten Albe and Till Frömling are thanked for discussions on dislocation structures in oxides. We are indebted to the Deutsche Forschungsgemeinschaft for funding this work under No. 414179371. Atsutomo Nakamura acknowledges the financial supports of JST PRESTO Grant Number JPMJPR199A and JSPS KAKENHI Grant Numbers JP19H05786 and JP18H03840, Japan. Ultra-high voltage electron microscopy (UHVEM) observations in this work were conducted in Nagoya Univ., supported by Nanotechnology Platform Program of

MEXT, Japan. We are grateful to Mr. K. Higuchi for technical assistance with UHVEM experiments.

Funding

Open Access funding enabled and organized by Projekt DEAL.

Declarations

Conflict of interest The authors declare no conflicts of interest.

Supplementary Information: The online version contains supplementary material available at <http://doi.org/10.1007/s10853-022-07405-3>.

Open Access This article is licensed under a Creative Commons Attribution 4.0 International License, which permits use, sharing, adaptation, distribution and reproduction in any medium or format, as long as you give appropriate credit to the original author(s) and the source, provide a link to the Creative Commons licence, and indicate if changes were made. The images or other third party material in this article are included in the article's Creative Commons licence, unless indicated otherwise in a credit line to the material. If material is not included in the article's Creative Commons licence and your intended use is not permitted by statutory regulation or exceeds the permitted use, you will need to obtain permission directly from the copyright holder. To view a copy of this licence, visit <http://creativecommons.org/licenses/by/4.0/>.

References

- [1] Adepalli KK, Yang J, Maier J, Tuller HL, Yildiz B (2017) Tunable oxygen diffusion and electronic conduction in SrTiO₃ by dislocation-induced space charge fields. *Adv Funct Mater* 27:1700243. <https://doi.org/10.1002/adfm.201700243>
- [2] Szot K, Rodenbücher C, Bihlmayer G, Speier W, Ishikawa R, Shibata N, Ikuhara Y (2018) Influence of dislocations in transition metal oxides on selected physical and chemical properties. *Crystals* 8:241. <https://doi.org/10.3390/cryst8060241>
- [3] Porz L, Frömling T, Nakamura A, Li N, Maruyama R, Matsunaga K, Gao P, Simons H, Dietz C, Rohnke M, Janek J, Rödel J (2020) Conceptual framework for dislocation-modified conductivity in oxide ceramics deconvoluting mesoscopic structure, core, and space charge exemplified for SrTiO₃. *ACS Nano* 15:9355–9367. <https://doi.org/10.1021/acsnano.0c04491>
- [4] Muhammad QK, Porz L, Nakamura A, Matsunaga K, Rohnke M, Janek J, Rödel J, Frömling T (2021) Self-doping by mechanically induced dislocations in bulk TiO₂. *Nano Energy* 85:105944. <https://doi.org/10.1016/j.nanoen.2021.105944>
- [5] Adepalli KK, Kelsch M, Merkle R, Maier J (2013) Influence of line defects on the electrical properties of single crystal TiO₂. *Adv Funct Mater* 23:1798–1806. <https://doi.org/10.1002/adfm.201202256>
- [6] Otsuka K, Matsunaga K, Nakamura A, Ji S, Kuwabara A, Yamamoto T, Ikuhara Y (2004) Effects of dislocations on the oxygen ionic conduction in yttria stabilized zirconia. *Mater Trans* 45:2042–2047. <https://doi.org/10.2320/matertrans.45.2042>
- [7] Sun LX, Marrocchelli D, Yildiz B (2015) Edge dislocation slows down oxide ion diffusion in doped CeO₂ by segregation of charged defects. *Nat Commun* 6:6294. <https://doi.org/10.1038/ncomms7294>
- [8] Kim SI, Lee KH, Mun HA, Kim HS, Hwang SW, Roh JW, Yang DJ, Shin WH, Li XS, Lee YH, Snyder GJ, Kim SW (2015) Dense dislocation arrays embedded in grain boundaries for high-performance bulk thermoelectrics. *Science* 348:109–114. <https://doi.org/10.1126/science.aaa4166>
- [9] Sun B, Haunschild G, Polanco C, Ju J, Lindsay L, Kobl-muller G, Koh YK (2019) Dislocation-induced thermal transport anisotropy in single-crystal group-III nitride films. *Nat Mater* 18:136–140. <https://doi.org/10.1038/s41563-018-0250-y>
- [10] Porz L, Klomp A, Fang X, Li N, Yildirim C, Detlefs C, Bruder E, Höfling M, Rheinheimer W, Patterson EA, Gao P, Durst K, Nakamura A, Albe K, Simons H, Rödel J (2021) Dislocation-toughened ceramics. *Mater Horiz* 8:1528–1537. <https://doi.org/10.1039/d0mh02033h>
- [11] Höfling M, Zhou X, Riemer LM, Buder E, Liu B, Zhou L, Goszewicz PB, Zhuo F, Xu B-X, Durst K, Tan X, Damjanovic D, Koruza J, Rödel J (2021) Control of polarization in bulk ferroelectrics by mechanical dislocation imprint. *Science* 372:961–964. <https://doi.org/10.1126/science.abe3810>
- [12] Messerschmidt U (2010) Dislocation dynamics during plastic deformation, vol 129. Springer, New York, NY, USA
- [13] Rice RW (1972) Deformation, recrystallization, strength, and fracture of press-forged ceramic crystals. *J Am Ceram Soc* 55:90–97. <https://doi.org/10.1111/j.1151-2916.1972.tb11217.x>

- [14] Merkel S, Wenk HR, Shu JF, Shen GY, Gillet P, Mao HK, Hemley RJ (2002) Deformation of polycrystalline mgo at pressures of the lower mantle. *J Geophys Res-Sol Ea* 107:2271. <https://doi.org/10.1029/2001jb000920>
- [15] Wright K, Price GD, Poirier JP (1992) High-temperature creep of the perovskites CaTiO_3 and NaNbO_3 . *Phys Earth Planet Inter* 74:9–22. [https://doi.org/10.1016/0031-9201\(92\)90064-3](https://doi.org/10.1016/0031-9201(92)90064-3)
- [16] Taeri S, Brunner D, Sigle W, Rühle M (2004) Deformation behaviour of strontium titanate between room temperature and 1800 K under ambient pressure. *Z Metallkd* 95:433–446
- [17] Amodeo J, Merkel S, Tromas C, Carrez P, Korte-Kerzel S, Cordier P, Chevalier J (2018) Dislocations and plastic deformation in MgO crystals: A review. *Crystals* 8:240. <https://doi.org/10.3390/cryst8060240>
- [18] Gilman JJ, Johnston WG (1962) Dislocations in lithium fluoride crystals. *Solid State Phys* 13:147–222
- [19] Wang ZC, Karato S, Fujino K (1993) High-temperature creep of single-crystal strontium-titanate (SrTiO_3)—a contribution to creep systematics in perovskites. *Phys Earth Planet Inter* 79:299–312. [https://doi.org/10.1016/0031-9201\(93\)90111-L](https://doi.org/10.1016/0031-9201(93)90111-L)
- [20] Nakamura A, Matsunaga K, Tohma J, Yamamoto T, Ikuhara Y (2003) Conducting nanowires in insulating ceramics. *Nat Mater* 2:453–456
- [21] Otsuka K, Kuwabara A, Nakamura A, Yamamoto T, Matsunaga K, Ikuhara Y (2003) Dislocation-enhanced ionic conductivity of yttria-stabilized zirconia. *Appl Phys Lett* 82:877–879. <https://doi.org/10.1063/1.1544440>
- [22] Groves GW, Kelly A (1963) Independent slip systems in crystals. *Phil Mag* 8:877–887. <https://doi.org/10.1080/14786436308213843>
- [23] Taylor GI (1938) Plastic strain in metals. In: Twenty-eighth may lecture to the institute of metals delivered May 5th 1938
- [24] Pelleg J (2017) Creep in ceramics, vol 241. Springer Nature, Berlin
- [25] Pelleg J (2014) Mechanical properties of ceramics, vol 213. Springer, Berlin
- [26] Rheinheimer W, Hoffmann MJ (2015) Non-arrhenius behavior of grain growth in strontium titanate: New evidence for a structural transition of grain boundaries. *Scripta Mater* 101:68–71. <https://doi.org/10.1016/j.scriptamat.2015.01.021>
- [27] Baurer M, Kungl H, Hoffmann MJ (2009) Influence of sr/ti stoichiometry on the densification behavior of strontium titanate. *J Am Ceram Soc* 92:601–606. <https://doi.org/10.1111/j.1551-2916.2008.02920.x>
- [28] Sternlicht H, Rheinheimer W, Dunin-Borkowski RE, Hoffmann MJ, Kaplan WD (2019) Characterization of grain boundary disconnections in SrTiO_3 part I: The dislocation component of grain boundary disconnections. *J Mater Sci* 54:3694–3709. <https://doi.org/10.1007/s10853-018-3096-4>
- [29] Singh D, Lorenzo-Martin M, Chen G, Gutierrez-Mora F, Routbort JL (2007) High-temperature deformation behavior in SrTiO_3 ceramics. *J Eur Ceram Soc* 27:3377–3384. <https://doi.org/10.1016/j.jeurceramsoc.2007.02.186>
- [30] Reed R (2006) The superalloys: Fundamentals and applications. Cambridge University Press, Cambridge
- [31] Heuer AH, Sellers DJ, Rhodes WH (1969) Hot-working of aluminum oxide. I. Primary recrystallization and texture. *J Am Ceram Soc* 52:468–474. <https://doi.org/10.1111/j.1151-2916.1969.tb09195.x>
- [32] Rösler J, Haders H, Bäker M (2019) Mechanical behavior of engineering materials. Springer, Berlin
- [33] Simpson LA, Merrett GJ (1974) Effect of annealing on fracture toughness, strength and microstructure of hot-pressed alumina. *J Mater Sci* 9:685–688. <https://doi.org/10.1007/Bf02387545>
- [34] Evans AG, Gilling D, Davidge RW (1970) Temperature-dependence of strength of polycrystalline MgO. *J Mater Sci* 5:187–197. <https://doi.org/10.1007/Bf00550995>
- [35] Barmore WL, Vandervo RR (1965) High-temperature plastic deformation of polycrystalline beryllium oxide. *J Am Ceram Soc* 48:499–505. <https://doi.org/10.1111/j.1151-2916.1965.tb14648.x>
- [36] Orowan E (1940) Problems of plastic gliding. *Proc Phys Soc* 52:8–22
- [37] Hull D, Bacon DJ (2011) Introduction to dislocations, 5th edn. Elsevier, Amsterdam
- [38] Brunner D (2008) Can the kink-pair theory apply for the yield stress of single crystalline SrTiO_3 at high temperatures? *Mater Sci Eng A* 483–484:521–524. <https://doi.org/10.1016/j.msea.2006.10.177>
- [39] Ritterbex S, Hirel P, Carrez P (2018) On low temperature glide of dissociated $\langle 110 \rangle$ dislocations in strontium titanate. *Phil Mag* 98:1397–1411. <https://doi.org/10.1080/14786435.2018.1438682>
- [40] Langdon TG, Pask JA (1971) Effect of microstructure on deformation of polycrystalline MgO. *J Am Ceram Soc* 54:240–246. <https://doi.org/10.1111/j.1151-2916.1971.tb12280.x>
- [41] Day RB, Stokes RJ (1966) Mechanical behavior of polycrystalline magnesium oxide at high temperatures. *J Am Ceram Soc* 49:345–350. <https://doi.org/10.1111/j.1151-2916.1966.tb13282.x>
- [42] Copley SM, Pask JA (1965) Deformation of polycrystalline MgO at elevated temperatures. *J Am Ceram Soc* 48:636–642. <https://doi.org/10.1111/j.1151-2916.1965.tb14695.x>

- [43] Warshaw SI, Norton FH (1962) Deformation behavior of polycrystalline aluminum oxide. *J Am Ceram Soc* 45:479–486. <https://doi.org/10.1111/j.1151-2916.1962.tb11038.x>

Publisher's Note Springer Nature remains neutral with regard to jurisdictional claims in published maps and institutional affiliations.